PERGAMON

International Journal of Solids and Structures 38 (2001) 3233–3249

INTERNATIONAL JOURNAL OF SOLIDS and STRUCTURES

www.elsevier.com/locate/ijsolstr

Conservation laws of the J_k-vector for microcrack damage in piezoelectric materials

Y.H. Chen *, T.J. Lu

Department of Engineering, University of Cambridge, Trumpington Street, Cambridge CB2 1PZ, UK

Received 26 October 1999; in revised form 26 September 2000

Abstract

This paper focuses on characterizing damaged anisotropic piezoelectric materials by using the principles of fracture mechanics. The interpretation and evaluation of the two components of the J_k-vector along contours enclosing strongly interacting microcracks in two-dimensional piezoelectric materials are presented. The conservation laws of the J_k-vector established by Budiansky and Rice (ASME J. Appl. Mech. 40 (1973) 201) for traditional non-piezoelectric materials and extended by Chen and Hasebe (Int. J. Fract. 89 (1998) 333) and Chen (Int. J. Solids Struct. 38 (2000a) 3193 and 38 (2000b) 3213) for interacting multiple cracks are reexamined for anisotropic piezoelectric materials containing interacting multiple cracks. The interaction problem for arrays of arbitrarily orientated and distributed microcracks subjected to mechanical and electrical loading is studied in detail. The contribution of the second component of the J_k-vector, evaluated in the local coordinate system that is attached to each microcrack, to the J_k-vector evaluated in the global coordinate system is calculated. It is found that the conservation laws of the J_k-vector are still valid in damaged piezoelectric materials, although in the present problem the elastic and electric fields are coupled which add complications to the original formulations by Budiansky and Rice. In other words, the total contributions from the microcracks to both components of the J_k-vector evaluated in the global system vanish, provided that the selected closed contour encloses all microcracks and/or discontinuities. © 2001 Published by Elsevier Science Ltd.

Keywords: Conservation laws; Microcrack damage; *J*-integral; Piezoelectric ceramics; Interacting cracks; Stress intensity factors; Electric displacement intensity factors; Crack shielding

1. Introduction

Cracks-like defects are abundant in piezoelectric materials, and have been the subject of intensive study in the past decade (Pak, 1990; Sosa, 1991, 1992; Suo et al. 1992; Pak and Tobin, 1993; Dunn, 1994; Park and Sun, 1995a,b; Sosa and Khutoryyansky, 1996; Shido et al. 1997; Chung and Ting, 1996; Heyer et al. 1998; Park et al. 1998; Xu and Rajapakse, 1999). Recently, Han and Chen (1999) developed a 'pseudo-traction-electric displacement' method to solve the problem of interacting multiple parallel cracks for transversely isotropic piezoelectric materials. It is shown that, due to crack interactions, the stress intensity

* Corresponding author. Fax: +86-29-3237910.
E-mail addresses: yhc22@eng.cam.ac.uk, tjl21@eng.cam.ac.uk (Y.H. Chen).

0020-7683/01/$ - see front matter © 2001 Published by Elsevier Science Ltd.
PII: S0020-7683(00)00376-0

factors (SIFs) at each crack tip are no longer independent of remote electric loadings, in contrary to those for single crack problems (Park and Sun, 1995a,b). The formation of multiple parallel cracks next to a single crack not only relaxes the residual stresses but also disturbs the electric field in the vicinity of the crack. It is the latter source that leads to the indirect but significant influence of electric loadings on the SIFs as well as on the mechanical-strain-energy release rate (MSERR). The work of Han and Chen (1999) is an initial attempt to solve the more general crack-interaction problems, as only the first component of the J_k-vector is concerned due to the assumption that the multiple cracks are parallel with each other and perpendicular to the poling direction of the piezoelectric ceramics. For multiple cracks arbitrarily oriented and distributed in a piezoelectric such that they are not necessarily perpendicular to the poling direction of the material, the role of electric loading is unclear. Moreover, the validity of the conservation laws of the J_k-vector in such situations needs to be established since Chen (2000a,b) has shown that the second component of the vector must be considered if the interacting cracks are no longer parallel.

This paper presents an analytical and numerical study of and conservation laws of the J_k-vector (Budiansky and Rice, 1973) and their application, for strongly interacting and arbitrarily oriented microcracks in two-dimensional (2-D) anisotropic piezoelectric materials. Following Suo et al. (1992), the physical interpretation of the second component of the J_k-vector in such materials is established. The problem is reduced to a system of integral equations, which are subsequently solved numerically by using the Chebyshev integration technique. The conservation laws of the J_k-vector established for non-piezoelectric materials (Budiansky and Rice, 1973; Chen and Hasebe, 1998) are reexamined for the present interacting problem in piezoelectric materials; numerical results for a PTZ-4 ceramic are given to complement the analytical work. It is found that the total contributions from a cloud of microcracks in 2-D piezoelectric materials to each component of the J_k-vector evaluated in a global system vanish, if the closed contour encloses all microcracks.

2. J_k-vector: physical interpretation and conservation laws

2.1. Path independence of J_k-vector

For a plane crack in a 2-D anisotropic piezoelectric material, the J-integral is given by (Suo et al., 1992):

$$J = \oint_C \left[\left(\frac{1}{2}\sigma_{ij}\varepsilon_{ij}\,\mathrm{d}x_2 - n_i\sigma_{ip}\frac{\partial u_p}{\partial x_1}\mathrm{d}s \right) - \left(\frac{1}{2}D_iE_i\,\mathrm{d}x_2 + n_iD_i\frac{\partial \phi}{\partial x_1}\mathrm{d}s \right) \right] \tag{1}$$

where C refers to a closed contour starting from one point on the lower surface of the crack and ending at another point on the upper surface of the crack, and σ_{ij}, ε_{ij}, u_p, D_i, E_i, and ϕ are the stresses, strains, displacements, electric displacements, electric field components, and electric potential, respectively. Here, $i, j, p = 1$ and 2, n_i is the outer normal to the contour C, and (x_1, x_2) is the Cartesian coordinate system.

By comparing Eq. (1) with the original interpretation of the J-integral by Rice (1968) for non-piezoelectric materials, it is seen that the first two terms in Eq. (1) contributed by the mechanical quantities are identical to those in Rice's formulation, and the last two terms are additional ones introduced to account for the contributions from the electric quantities. In other words, although the electric and mechanical quantities are coupled in the constitutive equations for piezoelectric materials (see e.g., Suo et al., 1992), they are not directly linked together in Eq. (1).

According to Budiansky and Rice (1973), the J-integral is only the first component of the J_k-vector ($k = 1, 2$), which is parallel to the crack surfaces and will be denoted below by J_1. The second component denoted by J_2 is perpendicular to the crack surfaces and can be introduced in a similar way as J_1:

$$J_2 = \oint_C \left[\left(-\frac{1}{2}\sigma_{ij}\varepsilon_{ij}\,\mathrm{d}x_1 - n_l\sigma_{lp}\frac{\partial u_p}{\partial x_2}\mathrm{d}s \right) - \left(-\frac{1}{2}D_iE_i\,\mathrm{d}x_1 + n_iD_i\frac{\partial \phi}{\partial x_2}\mathrm{d}s \right) \right] \tag{2}$$

Note that the J_2-integral is in general path-dependent when the integral contour C encloses only one single tip of a crack. It is therefore likely to be far from significant as it would be in brittle materials (Herrmann and Herrmann, 1981). However, recent investigations of Chen and Ma (1997) and Chen and Hasebe (1998) reveal that, for multiple crack interaction problems in traditional non-piezoelectric materials, the J_2-integral plays a role similar to that of J_1. This conclusion is reached by assuming, as suggested by Herrmann and Herrmann (1981), that the closed contour selected for calculating the J_2-integral encloses either one single crack completely or all cracks present in the material. Under this assumption, both components of the J_k-vector are then path independent and hence have equal physical significance.

2.2. Conservation laws: statement

The new conservation laws of the J_k-vector for a 2-D piezoelectric material containing one or more cracks/discontinuities can be stated as: the total contributions to both J_1- and J_2-integrals evaluated along a closed path C_0 (Fig. 1) enclosing either a single crack/discontinuity completely or all cracks/discontinuities vanish. Mathematically, this can be written as:

$$\sum_{l=1}^{N} J_{1(l)} = 0 \tag{3}$$

$$\sum_{l=1}^{N} J_{2(l)} = 0 \tag{4}$$

where N refers to the total number of cracks/discontinuities in the material, and the subscript l refers to the lth crack such that $J_{1(l)}$ and $J_{2(l)}$ denote the contributions of the lth crack to the first and second components of the J_k-vector evaluated in a global system (x_1, x_2). The contribution of the lth crack evaluated in a local system (x_1^l, x_2^l) to the J_k-vector, denoted separately by $J_{1(l)}^l$ and $J_{2(l)}^l$ (Fig. 1), are related to $J_{1(l)}$ and $J_{2(l)}$ by:

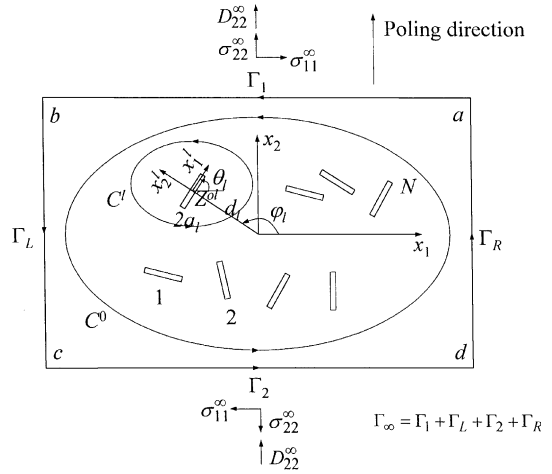

Fig. 1. Geometry and conventions for a cloud of randomly distributed and oriented interacting cracks in an infinite piezoelectric solid subjected to combined mechanical and electric loadings.

$$J_{1(l)} = J^l_{1(l)}\cos\theta_l - J^l_{2(l)}\sin\theta_l \tag{5}$$

$$J_{2(l)} = J^l_{1(l)}\sin\theta_l + J^l_{2(l)}\cos\theta_l \tag{6}$$

where the superscript l is used to denote quantities that are evaluated in the local system (x^l_1, x^l_2), and θ_l is the orientation angle of the crack measured from the x_1-axis to the x^l_1-axis (Fig. 1).

Eqs. (3)–(6) provide the new conservation laws of the J_k-vector in strongly interacting multiple crack problems for piezoelectric materials, which show quite different aspects from those customarily used in single crack problems for traditional non-piezoelectric materials (see, e.g., Rice, 1968, Budiansky and Rice, 1973, Herrmann and Herrmann, 1981). These have already been proved numerically (Chen and Hasebe, 1998) and analytically (Chen, 2000a) for non-piezoelectric brittle materials. Because Eqs. (5) and (6) are concerned with the projected relations of the J_k-vector between its values in the local system and those in the global system (Fig. 1), they may also be termed as *the projected conservation laws of the J_k-vector* for strongly interacting cracks in a 2-D solid. For anisotropic piezoelectric materials, the conservation laws (3)–(6) should be re-examined since the elastic and electric fields are coupled and the displacements and electric displacements add complications to the original formulations of the vector by Budiansky and Rice (1973).

2.3. Mathematical proof of conservation laws

2.3.1. Definition of problem and selection of boundary conditions

The multi-crack interacting problem to be solved is shown in Fig. 1, where N arbitrarily oriented microcracks are distributed in an infinitely large, two dimensional anisotropic piezoelectric solid. Assume that all the microcracks are fully open and not intersecting with each other, and that the distance between the center of a typical microcrack, say the lth microcrack, and that of its immediate neighbor is of the same order of magnitude as the average length of the microcracks. In other words, the space among the cracks may be smaller than the crack length. Therefore, strong interaction amongst the cracks is expected. With reference to Fig. 1, let a_l be the half-length of the lth microcrack, θ_l its orientation angle, ϕ_l its location angle, and let d_l denote the distance of the center of the lth microcrack to the origin of the global system (x_1x_2). The remote loading conditions are σ^∞_{22} and D^∞_2 along the x_2-axis and σ^∞_{12} along the x_1-axis. The poling direction of the piezoelectric material is taken to be parallel to the x_2-axis but may not always be perpendicular to the microcracks.

For a typical microcrack, three types of electric boundary condition may be used (Pak, 1992; Suo et al., 1992; Hao and Shen, 1994):

(i) Insulation boundary condition (charge free crack or impermeable crack):

$$D^+_n = D^-_n = 0 \tag{7}$$

(ii) Conduction boundary condition (permeable or continuous crack):

$$D^+_n = D^-_n, \quad \phi^+ = \phi^- \tag{8}$$

(iii) Mixed boundary condition:

$$D^+_n = D^-_n, \quad D^+_n(u^+_n - u^-_n) = \varepsilon_v(\phi^- - \phi^+) \tag{9}$$

where D^+_n and D^-_n are the upper and lower boundary values of the electric displacement on the crack, ϕ^+ and ϕ^- are the upper and lower boundary values of the electric potential on the crack, ε_v is the dielectric permittivity of the medium inside the crack (as a void), and u^+_n and u^-_n are the upper and lower boundary values of the displacement on the crack, respectively.

Since the mechanical and electric quantities are coupled and the three different types of crack boundary condition would lead to significantly different behaviors of the energy release rate (ERR), there has been considerable effort to find dominant parameters that govern crack stability and growth in piezoelectric ceramics. For example, Park and Sun (1995a,b) concluded that neither the SIF nor the J-integral $(=J_1)$ are suitable for describing the stability of an insulated crack; the MSERR was proposed as a new fracture parameter. In contrary, Heyer et al. (1998) performed a series of experimental measurements based on the conduction crack condition, and found that the SIF is still a suitable parameter to describe the stability of a conducting crack. On the other hand, Suo et al. (1992) argued that the permeable condition is not realistic as there is always an electric potential drop across a crack. More recently, Xu and Rajapakse (1999) developed a unified formulation for a crack containing either air or vacuum in piezoelectric ceramics. However, despite all these efforts, the true electric boundary condition on the crack surfaces remains an issue to be resolved, and is a topic beyond the scope of this paper. The purpose of this paper is not to clarify the confusion regarding the three types of electric boundary condition but rather to explore if there exist conservation laws in piezoelectric materials containing strongly interacting cracks. If the conservation laws indeed exist, these should be valid irregardless of the type of electric boundary condition selected. Consequently, unless otherwise stated, the insulation boundary condition (7) will be used throughout the remainder of this paper.

2.3.2. Mathematical proof

As there has been some doubt about the validity of Eqs. (3) and (4), a detailed proof is given below, the key being the correct use of the remote uniform stress-electric field. Introduce a closed but sufficiently large contour $\Gamma_\infty = \Gamma_1 + \Gamma_L + \Gamma_2 + \Gamma_R$ surrounding all the cracks, and introduce a smaller closed contour C_l which only encloses the lth crack completely (Fig. 1). According to the path-independent nature of the J_k-integral vector, one has

$$J_1^\infty = \sum_{l=1}^{N} J_{1(l)} \tag{10a}$$

$$J_2^\infty = \sum_{l=1}^{N} J_{2(l)} \tag{10b}$$

where the terms on the left hand side are calculated over Γ_∞, whilst the terms on the right hand side are calculated over C_l with $l = 1, 2, \ldots, N$. Since every term in the summation of Eq. (10a) or Eq. (10b) is in general not equal to zero due to strong interaction amongst the cracks, it is not clear whether the summation should vanish, or not, as a number of people have suspected.

In order to take full advantage of the remote uniform stress-electric field, the closed rectangular contour Γ_∞ has been chosen as large as possible. The reason to introduce the rectangular closed contour rather than an arbitrary one is to significantly simplify the mathematical manipulations involved. However, due to the path-independent nature of the vector, the results evaluated along an arbitrary smooth closed contour C_0 (be it large or small, see Fig. 1) should be identical to those calculated over Γ_∞. It is worth mentioning here that the second component of the vector is also path-independent, because the closed contour is always chosen either to enlose all the cracks or to enclose a single crack completely (Herrmann and Herrmann, 1981).

Since the traction-free surfaces of each crack lead to non-zero contributions to the second component (Herrmann and Herrmann, 1981), the three different types of electric boundary condition will also lead to non-zero contributions to the last two terms of Eq. (2). Of course, different electric conditions are expected to yield different magnitudes of these contribution, but the path-independent nature of the integral should

not be altered if the closed contour is chosen as C_l (Fig. 1). A universal formulation for a typical crack l in its local coordinate system (x_1^l, x_2^l) with θ_l as the orientation angle can always be written as

$$F_{2al}^{*} = \int_{-a_l}^{a_l} \left[\left(w_{\mathrm{m}}^{+} - w_{\mathrm{m}}^{-} \right) + \left(w_{\mathrm{e}}^{+} - w_{\mathrm{e}}^{-} \right) \right] \mathrm{d}x_{1^*}^{(l)} \tag{11}$$

where F_{2al}^{*} represents the contribution from the surfaces of the lth crack, the superscripts + and − denote the upper and lower boundary values on the crack surfaces, and the subscripts m and e refer to the mechanical energy and electric energy, respectively, given by:

$$W_{\mathrm{m}} = \tfrac{1}{2}\sigma_{ij}\varepsilon_{ij} \tag{12a}$$

$$W_{\mathrm{e}} = -\tfrac{1}{2}D_i E_i \tag{12b}$$

Eq. (11) and Eqs. (12a) and (12b) will be calculated below by using a technique developed specially for the current situation.

Since $\mathrm{d}y = \mathrm{d}x_2 = 0$ on Γ_1 and Γ_2, and $\mathrm{d}x = \mathrm{d}x_1 = 0$ on Γ_{L} and Γ_{R}, the left side of Eq. (10a) becomes

$$\begin{aligned} J_1^{\infty} = & \int_{\Gamma_1+\Gamma_2} \left[(-\sigma_{i2}^{\infty} n_2 \partial u_i/\partial x) + (-D_2 n_2 \partial \phi/\partial x) \right] \mathrm{d}s + \int_{\Gamma_{\mathrm{L}}+\Gamma_{\mathrm{R}}} (W_{\mathrm{m}} + W_{\mathrm{e}})\, \mathrm{d}y \\ & + \int_{\Gamma_{\mathrm{L}}+\Gamma_{\mathrm{R}}} \left[(-\sigma_{i1} n_1 \partial u_i/\partial x) + (-D_1 n_1 \partial \phi/\partial x) \right] \mathrm{d}s \end{aligned} \tag{13}$$

With that $n_2 = 1$ on Γ_1, $n_2 = -1$ on Γ_2, $n_1 = 1$ on Γ_{R} and $n_1 = -1$ on Γ_{L}, (13) can be rewritten as

$$\begin{aligned} J_1^{\infty} = & \sigma_{i2}^{\infty} \left[\int_a^b u_{i,1} \mathrm{d}x - \int_d^c u_{i,1} \mathrm{d}x \right] + D_2^{\infty} \left[\int_a^b \phi_{,1} \mathrm{d}x - \int_d^c \phi_{,1} \mathrm{d}x \right] \\ & + \left[\frac{1}{2} \sigma_{ij}^{\infty} \varepsilon_{ij}^{\infty} \left(\int_b^c \mathrm{d}y - \int_a^d \mathrm{d}y \right) \right] - \left[\frac{1}{2} D_i^{\infty} E_i^{\infty} \left(\int_b^c \mathrm{d}y - \int_a^d \mathrm{d}y \right) \right] \\ & + \sigma_{i1}^{\infty} \left[\int_b^c u_{i,1} \mathrm{d}y - \int_a^d u_{i,1} \mathrm{d}y \right] + D_1^{\infty} \left[\int_b^c \phi_{,1} \mathrm{d}y - \int_a^d \phi_{,1} \mathrm{d}y \right] \end{aligned} \tag{14}$$

Obviously, the third and forth terms in Eq. (14) vanish because $[\int_b^c \mathrm{d}y - \int_a^d \mathrm{d}y] = 0$, whereas the first term depends on the value of $[\int_a^b u_{i,1}\mathrm{d}x - \int_d^c u_{i,1}\mathrm{d}x]$, the second term on the value of $[\int_a^b \phi_{,1}\mathrm{d}x - \int_d^c \phi_{,1}\mathrm{d}x]$, the fifth term on the value of $[\int_b^c u_{i,1}\mathrm{d}y - \int_a^d u_{i,1}\mathrm{d}y]$, and the sixth term on the value of $[\int_b^c \phi_{,1}\mathrm{d}y - \int_a^d \phi_{,1}\mathrm{d}y]$. It should be mentioned that $u_{i,1}$ and $\phi_{,1}$ in the integrals are defined at infinity since the rectangular closed contour has been chosen as large as possible.

Now, the remote displacement field must be linear with respect to both x- and y-coordinates so that the uniform strain field at infinity would be maintained. Similarly, the electric potential should also be linear in order that the uniform electric displacement field at infinity is sustained. In fact, the remote uniform mechanical-electric fields do not depend on the configuration of the N interacting cracks, even if the array of the cracks is not symmetrical with respect to either $x = 0$ or $y = 0$. Therefore, the asymptotic values of $u_{i,1}$ at infinity should be constant, i.e., the integral $\left[\int_a^b u_{i,1}\mathrm{d}x - \int_d^c u_{i,1}\mathrm{d}x\right]$ should vanish. Similarly, the asymptotic values of $\phi_{,1}$ at infinity should also be constant and hence the integral $\left[\int_a^b \phi_{,1}\mathrm{d}x - \int_d^c \phi_{,1}\mathrm{d}x\right]$ vanishes.

The situation becomes much more clearer when the original problem shown in Fig. 1 is divided into two sub-problems. The first involves no cracks, with linear remote displacement and electric potential fields with respect to both x- and y-coordinates; the second involves N cracks with self-balanced tractions as well as self-balanced electric displacements acting on both surfaces of each individual crack, and no remote loading is applied. The detailed configuration of such subdivision is well-known, and hence is not repeated here. It suffices to mention that the second sub-problem yields zero displacement field at infinity because the stresses

and strains caused by the self-balanced surface tractions have an asymptotic nature with the order of r^{-2} (for large values of $r = \sqrt{x^2 + y^2}$). Thus, the remote displacement field is only dominated by the first sub-problem, resulting in $u_{i,1}(on\ \Gamma_1) = u_{i,1}(on\ \Gamma_2)$. A similar result holds for the electric field at infinity. These results leads directly to the conclusion that the first, second, fifth and sixth terms in Eq. (14) should all vanish, no matter how many cracks are present in the finite region of an infinite 2-D piezoelectric solid and whether the array of the cracks is symmetrical with respect to $x = 0$ (or $y = 0$) or not. Therefore, Eq. (3) as a new conservation law of the $J_1(= J)$ integral has been proved. Its validity will be confirmed further in Section 3 using numerical examples. Similarly, a straightforward manipulation can be given for Eq. (4) representing a new conservation law of the J_2 integral. For brevity, details are not repeated here.

Obviously, such vanishing nature of the vector does not depend on the shape of the cracks enclosed by the closed contour C_0 (Fig. 1). Therefore, other types of discontinuity such as curved cracks, bifurcated cracks, voids with arbitrary shapes, and inclusions, all enclosed by the contour C, will also satisfy Eqs. (3) and (4). The detailed expressions of the contributions from different types of discontinuity to the vector may of course be different, but the total summation of the contributions should vanish. It is important to note that the manipulations performed hitherto are independent upon the type of the electric boundary condition imposed on the crack surfaces. In other words, the conservation laws are always valid, irregardless of the type of electric boundary condition selected.

3. Numerical examples

To prove the conservation laws with numerical examples, an initial attempt has been made by Han and Chen (1999) who considered parallel microcracks oriented in a direction perpendicular to the poling direction of a transversely isotropic piezoelectric material. Therefore, only the J_1-integral is calculated since the contribution of $J^l_{2(l)}$ to $J_{1(l)}$ in Eq. (5) vanishes due to the fact that the orientation angle $\theta_l \equiv 0$ for this simple array of cracks.

For the problem shown in Fig. 1, the situation is much more complicated than that considered by Han and Chen (1999). The randomly oriented and distributed microcracks are no longer parallel with each other; they also are not necessarily perpendicular to the poling direction of the material. It is then expected that the $J^l_{2(l)}$ integral in the local system will play an important role as it would be in non-piezoelectric materials (Chen, 2000a). Before this can be verified, it is important to first find an accurate method to calculate numerically $J^l_{2(l)}$ in the local coordinate system (x^l_1, x^l_2), since Herrmann and Herrmann (1981) have shown that, besides the two crack tips of the lth microcrack, the traction-free surfaces of the lth microcrack also contribute to $J^l_{2(l)}$. Such a method is introduced below.

To calculate $J^l_{2(l)}$, a typical crack of length $2a_l$ is shown in Fig. 2 in a local coordinate system, where a special closed contour is introduced:

$$C_l = C_l^- + C_l^{\mathrm{R}} - C_l^+ - C_l^{\mathrm{L}} \tag{15}$$

where the superscripts + and − refer to the upper and lower surfaces of the crack, R and L refer to the right and left tips of the crack, and C_l^{R} and C_l^{L} denote two infinitely small circles with the radius $\rho \to 0$ (Fig. 2), respectively.

The calculation of $J^l_{2(l)}$ along C_l can be divided into two parts, one contributed by both tips of the crack along path C_l^{R} and C_l^{L}, and the other induced from the crack surfaces along path C_l^+ and C_l^-. The special technique proposed by the present authors and co-workers (Chen and Ma, 1997) for anisotropic elastic materials is adopted here. The integration of J^l_2 along an infinitely small circle surrounding a crack tip may be obtained by using the following ERR relationship (Chen and Ma, 1997):

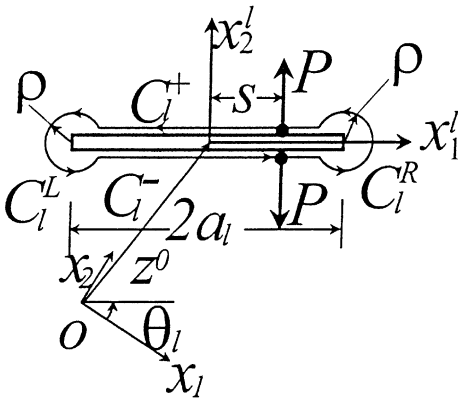

Fig. 2. Special closed contour for a single crack in local coordinates.

$$J_2^l = -g = \lim_{\Delta \to 0} \frac{-1}{2\Delta} \int_0^{\Delta} \sigma_{i1}(\Delta - \rho) u_i(\rho)\, \mathrm{d}\rho \quad (i = 1, 2) \tag{16}$$

where J_2^l refers to the contribution from a single crack tip to the J_2-integral and g denotes the ERR as defined by Chen and Ma (1997).

The validity of Eq. (16) will be checked against numerical results presented below. As regards the contribution of both surfaces of the crack to $J_{2(l)}^l$, there are no special difficulties to be overcome as long as all mechanical and electric quantities along C^+ and C^- are known a priori. It will be shown in Section 3.1 that these quantities can be determined by employing the complex function method and performing the Chebyshev numerical integration.

3.1. Pseudo-traction-electric-displacement method

The interaction problem among N cracks in an anisotropic piezoelectric material (Fig. 1) can be solved by extending the pseudo-traction method developed by Horii and Nemat-Nasser (1985, 1987) for solving multiple crack interaction problems in non-piezoelectric materials. The key here is to decompose the original problem into N sub-problems, each containing one single crack with pseudo-tractions and pseudo-electric-displacement assigned to both of its surfaces. Once the fundamental solutions for a single crack loaded by concentrated tractions and concentrated electric displacement on both crack surfaces are found, the following set of Fredholem integral equations can be derived from simple superposition (Han and Chen, 1999):

$$\mathbf{P}^l(s) + \sum_{j=0}^{N} \sigma^{lj}(s) = 0 \quad (l = 1, 2, 3, \ldots, N, j \neq l) \tag{17}$$

Here, $\mathbf{P}^l(s)$ denotes a function vector with the unknown pseudo-tractions and electric-displacement on both surfaces of the lth crack as its elements, and $\sigma^{l0}(s)$ refers to the stresses and electric displacement arising from the remote loading σ^{∞} and D_2^{∞}, given by

$$\sigma^{l0}(s) = \mathbf{R}_1 \sigma^{\infty} \tag{18}$$

where

$$\sigma^{\infty} = [\sigma_{12}^{\infty}, \sigma_{22}^{\infty}, 0, D_2^{\infty}]^{\mathrm{T}} \tag{19}$$

$$\mathbf{R}_1 = \begin{bmatrix} \frac{1}{2}\cos 2\theta & \frac{1}{2}\sin 2\theta & 0 & 0 \\ -\frac{1}{2}\sin 2\theta & \cos^2\theta & 0 & 0 \\ 0 & 0 & \cos\theta & 0 \\ 0 & 0 & 0 & \cos\theta \end{bmatrix} \tag{20}$$

Furthermore, in Eq. (17), $\sigma^{lj}(s)$ denotes the contribution of the rest of the microcracks to the lth crack:

$$\sigma^{lj}(s) = \int_{-a_l}^{a_l} \mathbf{F}^{lj}(s,x)\mathbf{P}^{j}(X)\,\mathrm{d}x \quad (j \neq l) \tag{21}$$

where

$$\mathbf{P}^{J}(x) = [P_1^J(x), P_2^j(x), P_3^j(x), D_2^j(x)]^{\mathrm{T}} \tag{22}$$

and $\mathbf{F}^{li}(s,x)$ is the influence function on the lth crack induced from the jth crack (Han and Chen, 1999).

The integral equation (17) can be solved numerically by expanding $\mathbf{P}^{(l)}(s)$ into the second Chebyshev polynomial:

$$\mathbf{P}^{l}(s) = \sum_{k=0}^{M} \mathbf{G}_k^l \mathbf{U}_k(s/a_l) \tag{23}$$

where

$$\mathbf{G}_k^l = \int_{-1}^{1} 2\sqrt{1-s^2}\mathbf{P}^l(a_l x)\mathbf{U}_k(x)/\pi\,\mathrm{d}x \tag{24}$$

and $\mathbf{U}_k(s/a_l)$ is the second Chebyshev polynomial with order k, and M is an integer number controlling the numerical accuracy.

Once Eq. (17) is solved, the SIFs and the electric displacement intensity factor (EDIF) at the right and left tips of the lth crack can be straightforwardly calculated as:

$$\mathbf{K}^{l\mathrm{R}} = -\int_{-a_l}^{a_l} \mathbf{P}^l(s)(a_l+s)^{1/2}(a_l-s)^{-1/2}(\pi a_l)^{-1/2}\mathrm{d}s \tag{25}$$

$$\mathbf{K}^{l\mathrm{L}} = -\int_{-a_l}^{a_l} \mathbf{P}^l(s)(a_l-s)^{1/2}(a_l+s)^{-1/2}(\pi a_l)^{-1/2}\mathrm{d}s \tag{26}$$

$$\text{where} \quad \mathbf{K}^{l\mathrm{R}} = [K_{\mathrm{II}}^{l\mathrm{R}}, K_{\mathrm{I}}^{l\mathrm{R}}, K_{\mathrm{III}}^{l\mathrm{R}}, K_{\mathrm{e}}^{l\mathrm{R}}] \tag{27}$$

$$\mathbf{K}^{l\mathrm{L}} = [K_{\mathrm{II}}^{l\mathrm{L}}, K_{\mathrm{I}}^{l\mathrm{L}}, K_{\mathrm{III}}^{l\mathrm{L}}, K_{\mathrm{e}}^{l\mathrm{L}}] \tag{28}$$

Here, the subscripts I, II, and III refer to the Mode I, Mode II, and Mode III SIFs, respectively, the subscript e denotes to the EDIF, and the subscripts l, R, and L represent separately the lth crack, its right and left tips.

The first component of the J_k-vector evaluated in the local coordinate system (x_1^l, x_2^l) origined at the center of the lth crack can be calculated as (see, for example, Suo et al. 1992)

$$J_1^{l\mathrm{R}} = \frac{1}{4}(\mathbf{K}^{l\mathrm{R}})^{\mathrm{T}}\mathbf{H}\mathbf{K}^{l\mathrm{R}} \tag{29}$$

$$J_1^{l\mathrm{L}} = \frac{1}{4}(\mathbf{K}^{l\mathrm{L}})^{\mathrm{T}}\mathbf{H}\mathbf{K}^{l\mathrm{L}} \tag{30}$$

On the other hand, from Eq. (16), it can be shown that the second component is given by:

$$J_2^{l\mathrm{R}} = \tfrac{1}{4}(\mathbf{K}^{l\mathrm{R}})^{\mathrm{T}}\mathbf{X}\mathbf{H}\mathbf{K}^{l\mathrm{R}} \tag{31}$$

$$J_2^{l\mathrm{L}} = -\tfrac{1}{4}(\mathbf{K}^{l\mathrm{L}})^{\mathrm{T}}\mathbf{X}\mathbf{H}\mathbf{K}^{l\mathrm{L}} \tag{32}$$

where the matrix $\mathbf{H}$ is

$$\mathbf{H} = 2\mathrm{Re}(\mathrm{i}\mathbf{A}\mathbf{B}^{-1}) \tag{33}$$

for which the matrices $\mathbf{X}$, $\mathbf{A}$, and $\mathbf{B}$ can be found in Suo et al. (1992).

Note that $J_2^{l\mathrm{R}}$ and $J_2^{l\mathrm{L}}$ only represent contributions of the right and left tips of the lth crack to $J_{2(l)}^l$ in the local coordinate system (x_1^l, x_2^l); they are calculated along C_l^{R} and C_l^{L} as $\rho \to 0$ (Fig. 2). To calculate the full value of $J_{2(l)}^l$, the contribution from both surfaces C_l^+ and C_l^- must included. However, since the integral equation (17) has already been solved numerically so that all the mechanical and electric quantities on the surfaces of the lth crack are now determined, the contribution of crack surfaces can be calculated numerically by using Eq. (11). Finally, the total contribution of the lth crack to the second component of the J_k-vector in the local coordinate system (x_1^l, x_2^l) is obtained as

$$\begin{aligned} J_{2(l)}^l &= J_2^{l\mathrm{R}} + J_2^{l\mathrm{L}} + J_2^{l\mathrm{f}} \\ &= \frac{1}{4}(\mathbf{K}^{l\mathrm{R}})^{\mathrm{T}}\mathbf{X}\mathbf{H}\mathbf{K}^{l\mathrm{R}} - \frac{1}{4}(\mathbf{K}^{l\mathrm{L}})^{\mathrm{T}}\mathbf{X}\mathbf{H}\mathbf{K}^{l\mathrm{L}} + \int_{-a_l}^{a_l}(W^+ - W^-)\,\mathrm{d}s \end{aligned} \tag{34}$$

The contribution of the lth crack to the vector in the global system can then be evaluated by using the projected relations (5) and (6).

3.2. Numerical results

Although the results presented above are derived for general anisotropic piezoelectric materials, for simplicity, the numerical results to be given below will be limited to a transversely isotropic piezoelectric material, i.e., the PTZ-4 ceramic, with its material constants given in Table 1. It is assumed that the poling direction of the ceramic is parallel to the x_2-axis (Fig. 1).

First, the formulation for calculating the J_2-integral induced only from one tip of a single crack embedded in the PTZ-4 ceramic is examined. Table 2 shows that the values derived by using Eq. (2) coincide well with those derived by using the ERR relation (16), no matter how the Mode I and Mode II SIFs and the EDIF at infinity are combined. Judging from the results of Table 2, one may conclude that the derivative procedure, i.e., Eq. (16), is not only valid for anisotropic elastic materials (Chen and Ma, 1997), but also valid for transversely isotropic piezoelectric ceramics.

The conservation laws of the J_k-vector, i.e., Eqs. (3) and (4), are examined next by introducing an array of four microcracks (Fig. 3), each of length $2a$, with orientations and locations specified in Table 3. Here, d_l, φ_l, θ_l, and $x_{1(l)}$, and $x_{2(l)}$ ($l = 1, 2, 3,$ and 4) denote separately the location distance from the origin, location

Table 1
Material constants of PTZ-4 ceramics

C_{11}	C_{12}	C_{13}	C_{33}	C_{44}	Unit
1.4020	0.7892	0.7565	1.1577	0.2525	$(\mathrm{N/m^2}) \times 10^{11}$
e_{31}	e_{33}	e_{15}			
−5.2677	15.4455	12.0000			$(\mathrm{C/m^2})$
w_{11}	w_{33}				
0.6359	0.5523				$(\mathrm{C/Vm}) \times 10^{-8}$

Table 2
Numerical examination for the J_2-integral (2) and the ERR g in Eq. (16) under combined mechanical and electric loading conditions

K_{II}/K_I	K_1/K_I	K_{III}/K_I	K_e^N	$r = 0.1$		$r = 1.0$	
				J_2^t/J_1	$-g/J_1$	J_2^t/J_1	$-g/J_1$
0.5	0.5	0.0	0.0	1.31667	1.31667	1.31667	1.31667
0.5	1.0	0.0	0.0	1.06462	1.06462	1.06462	1.06462
1.0	0.5	0.0	0.0	1.04227	1.04227	1.04227	1.04227
0.5	0.5	0.0	1.0	−0.18119	−0.18119	−0.18119	−0.18119
1.0	1.0	0.0	1.0	−5.37522	−5.37522	−5.37522	−5.37522

($K_e^N = K_e/(10^{-8}K_I CN^{-1})$).

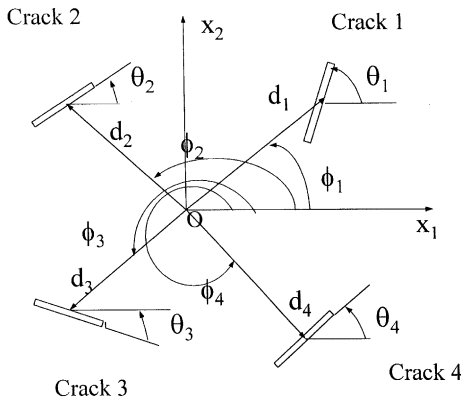

Fig. 3. Geometry and conventions for four interacting cracks.

Table 3
Orientations and relative positions of four microcracks

l	1	2	3	4
θ_l	Variable	−25°	55°	30°
φ_l	45°	140°	260°	340°
d_l	1.6a	1.4a	1.3a	1.6a
$x_{1(l)}$	1.1314a	−1.0725a	−0.2257a	1.5035a
$x_{2(l)}$	1.1314a	0.9000	−1.2803a	−0.5472a

angle, orientation angle, and position coordinates of the center of the lth microcrack in the global coordinate system (x_1, x_2). Without loss of generality, three types of remote loading condition are considered: (i) pure Mode I mechanical loading, with $\sigma_{12}^{\infty} = \sigma_{32}^{\infty} = D_2^{\infty} = 0$ and $\sigma_{22}^{\infty} > 0$; (ii) Mode I mechanical loading combining with positive electric loading, with $\sigma_{12}^{\infty} = \sigma_{32}^{\infty} = 0$, $\sigma_{22}^{\infty} > 0$, and $D_2^{\infty} = 10^{-8}\sigma_{22}^{\infty}C/N$; (iii) Mode I mechanical loading combining with negative electric loading, with $\sigma_{12}^{\infty} = \sigma_{32}^{\infty} = 0$, $\sigma_{22}^{\infty} > 0$, and $D_2^{\infty} = -10^{-8}\sigma_{22}^{\infty}C/N$. Numerical experiments reveal that a value of 41 for the total number of terms M in the Chebyshev polynomial (23) yields satisfactory accuracy for all three types of remote loading condition; $M = 41$ is therefore used in all subsequent numerical calculations.

For type (ii) remote loading condition (Mode I mechanical loading combining with positive electric loading), Table 4 shows the values of $J_{1(l)}$ $(l = 1, 2, 3, 4)$ contributed by the four microcracks to the J-integral. Here, the J_k-vector is normalized by

Table 4
Values of $J_{1(l)}/J_0$ $(l = 1, 2, 3, 4)$ under combined mechanical and positive electric loading (type (ii) loading)

θ_1	0°	30°	60°	90°	120°	150°
$J_{1(1)}/J_0$	−0.0200	−0.2377	−0.0594	0.0032	−0.0536	−0.0020
$J_{1(2)}/J_0$	−0.0123	0.2293	0.0475	−0.0415	−0.0824	−0.0993
$J_{1(3)}/J_0$	0.0763	0.0960	0.1401	0.1278	0.0964	0.0774
$J_{1(4)}/J_0$	−0.0439	−0.0875	−0.1282	−0.0895	0.0396	0.0239
$\sum J_{1(l)}/J_0$	0.0000	0.0000	0.0000	0.0000	0.0000	0.0000

Table 5
Values of $J_{2(l)}/J_0$ $(l = 1, 2, 3, 4)$ under combined mechanical and negative electric loading (type (iii) loading)

θ_1	0°	30°	60°	90°	120°	150°
$J_{2(1)}/J_0$	−0.1308	−0.0281	0.1020	0.0114	−0.0121	0.0144
$J_{2(2)}/J_0$	0.2673	0.1305	−0.0379	−0.0074	0.0386	0.1247
$J_{2(3)}/J_0$	−0.2342	−0.2310	−0.2538	−0.2831	−0.2639	−0.2419
$J_{2(4)}/J_0$	0.0977	0.1286	0.1897	0.2791	0.2374	0.1028
$\sum J_{2(l)}/J_0$	0.0000	0.0000	0.0000	0.0000	0.0000	0.0000

$$J_0 = \frac{1}{4}(\mathbf{K}_0)^{\mathrm{T}}\mathbf{H}_0\mathbf{K}_0 \tag{35}$$

where $\mathbf{K}_0$ and $\mathbf{H}_0$ are the fundamental solutions for a single crack, oriented parallel to the x_1-axis, subjected to the same type (ii) loading condition. The orientation angle θ_1 of the first microcrack in Table 3 is taken to be 0°, 30°, 60°, 90°, 120°, and 150°, respectively. It is seen from Table 4 that the summation of $J_{1(l)}$ $(l = 1, 2, 3, 4)$ indeed vanishes, confirming the conservation law (3). Table 5 presents the numerical results for $J_{2(l)}$ under type (iii) loading condition (Mode I mechanical loading combining with the negative electric loading). Again, the summation of $J_{2(l)}$ $(l = 1, 2, 3, 4)$ is seen to vanish, as suggested by the conservation law (4). Thus, the conservation laws of the J_k-vector (3) and (4) for non-piezoelectric materials (Chen and Hasebe, 1998; Chen, 2000a) have been shown to be equally valid for multiple crack interaction problems in piezoelectric materials. That is, the summation of the contributions induced from all the microcracks to each component of the J_k-vector always vanishes, even though the values of $J_{1(l)}$ and $J_{2(l)}$ for each individual microcrack are far from zero due to strong crack interactions. Consequently, the conservation laws as formulated by Eqs. (3) and (4) provide not only a consistency check of the numerical results presented in this section but also a powerful tool to examine the validity of the 'pseudo-traction-electric-displacement' method developed in Section 3.1.

4. Applications: two arbitrarily located interacting cracks

In this section, the pseudo-traction-electric-displacement method is used to study in detail the interaction effect between two arbitrarily located microcracks (Fig. 4) on crack tip parameters such as SIFs and EDIF. The two cracks are embedded in an infinitely large PTZ-4 ceramic. Crack 1 is always parallel to the global coordinate axis x_1, whereas the position and orientation of crack 2 with respect to crack 1 are arbitrary. Let $2a$ denote the length of the microcracks, and let θ_2, ϕ_2 and d_{12} represent the orientation angle, location angle, and distance from tip A of crack 1 to the center O_2 of crack 2, respectively. For illustration, the normalized distance between the two crack centers is taken as $d_{12}/a = 1.2$, the orientation angle of crack 2 is assumed to be $\phi_2 = 60°$, whilst the location angle of crack 2, θ_2, varies from 0° to 180°. All three types of

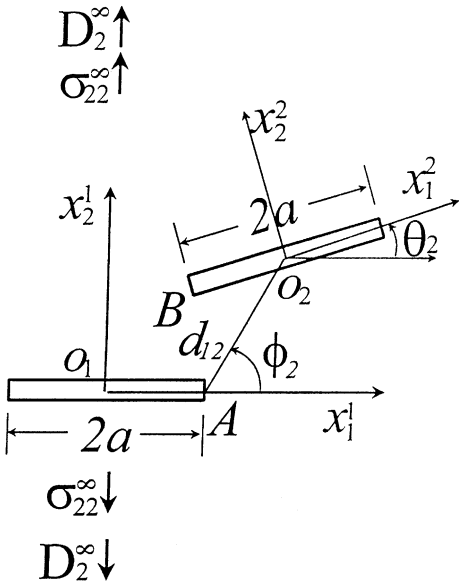

Fig. 4. Geometry and conventions for two arbitrarily located and oriented interacting cracks.

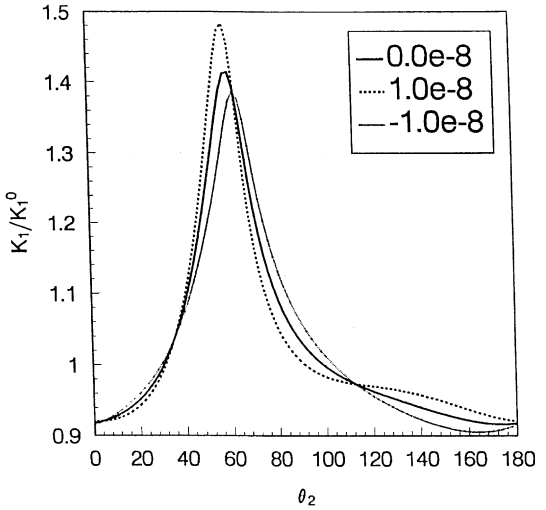

Fig. 5. Normalized Mode I SIF at tip A of crack 1, K_1/K_1^0, plotted as a function of its orientation angle of crack 2, θ_2, for type (i), (ii), and (iii) loading conditions ($D_2^\infty/\sigma_{22}^\infty = 0$, 10^{-8}, $-10^{-8}C/N$, respectively).

remote loading condition discussed in the previous sections are examined, with $D_2^\infty/\sigma_{22}^\infty = 0$, 10^{-8}, $-10^{-8}C/N$, respectively.

Fig. 5 plots the normalized Mode I SIF at the tip A of crack 1 (see Fig. 4) as a function of the location angle θ of crack 2 for types (i), (ii), and (iii) loading conditions. Although the trends are in general similar, there is considerable deviation of the dotted lines corresponding to types (ii) and (iii) loading conditions from the solid line corresponding to the pure mechanical loading (type (i)). Moreover, the positive electric loading (type (ii)) and negative electric loading (type (iii)) have opposite effects on the SIF. That is, for

certain values of θ_2, e.g., the range between 3° and 34° or the range between 63° and 112°, the positive electric loading tends to decrease the SIF whereas the negative electric loading tends to increase the SIF. For other ranges of θ_2, e.g., the range between 34° and 62° or the range between 112° and 180°, the roles of the positive and negative electric loading reverse. Four electric-neutral angles (ENA), 3°, 34°, 63° and 112°, can be identified on Fig. 5, where neither positive nor negative electric loading influences the value of SIF.

Of great interest is the influence of remote electric loading on the position of the maximum interacting effect angle (MIEA) (Fig. 5), which is defined here as the location angle of crack 2 that leads to the maximum interacting effect between the two cracks. Fig. 5 suggests that the electric loading shifts the value of MIEA, which is about 60° under pure mechanical loading (type (i)): a positive electric loading decreases MIEA but increases the crack interaction effect; a negative electric loading increases MIEA whereas reduces the interacting effect. These are apparently non-linear effects of the electric loading on SIF. In other words, although the positive and negative electric loadings have opposite effects on SIF, the effects are not proportional. Fig. 6 presents the normalized Mode I SIF at the tip B of crack 2 as a function of θ. The trends are similar to those discussed above for Fig. 5.

The results shown in Figs. 5 and 6 for the two interacting cracks problem are quite different from those given in Sosa (1991, 1992) for the single crack problem. Sosa (1991, 1992) found that the remote electric loading has no influence on the Mode I SIF at the tip of a single crack embedded in an infinitely large piezoelectric solid. In the present problem with two interacting cracks, the second crack centered at O_2 (Fig. 4) not only releases stresses in the vicinity of tip A of the first crack centered at O_1, but also disturbs the near-tip electric field at A. Similarly, the stress and electric fields in the vicinity of tip B of crack 2 are disturbed by the presence of crack 1. These are believed to be the reasons behind the coupling between electric loading and Mode I SIF for strongly interacting cracks.

The EDIF at crack tips A and B are shown in Figs. 7 and 8 as functions of θ, respectively. Again, it is seen that the positive and negative electric loadings have opposite effects on EDIF. However, in contrast to the case of Mode I SIF (Figs. 5 and 6), their influence on EDIF is apparently proportional because the mechanical loading has little influence on EDIF (see the solid lines in Figs. 7 and 8). The maximum influence of remote electric loading on EDIF occurs at about 62° for tip A (Fig. 7) and at about 55° for tip B (Fig. 8). Moreover, the influence of electric loading on EDIF depends strongly upon the orientation of the second crack. An electric neutral angle of about 90°, at which neither positive nor negative electric loading has influence on the EDIF at tip B, is seen to exist in Fig. 8. It corresponds to the case that crack 2 is

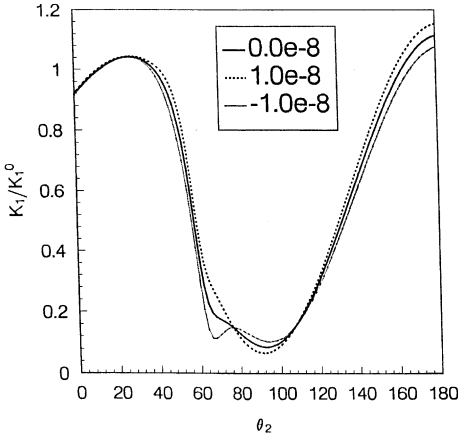

Fig. 6. Normalized Mode I SIF at tip B of crack 2, K_I/K_I^0, plotted as a function of its orientation angle of crack 2, θ_2, for type (i), (ii), and (iii) loading conditions ($D_2^\infty/\sigma_{22}^\infty = 0$, 10^{-8}, $-10^{-8}C/N$, respectively).

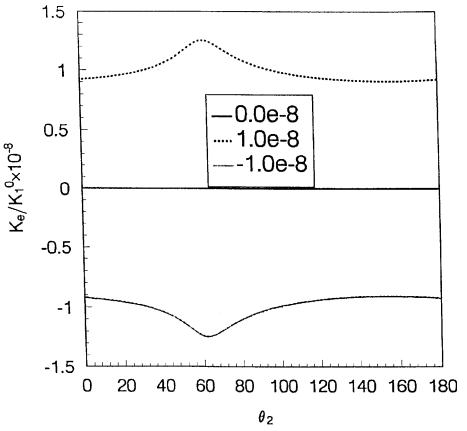

Fig. 7. Normalized EDIF at tip A of crack 1, K_e/K_I^0, plotted as a function of its orientation angle of crack 2, θ_2, for type (i), (ii), and (iii) loading conditions ($D_2^\infty/\sigma_{22}^\infty = 0$, 10^{-8}, $-10^{-8}C/N$, respectively).

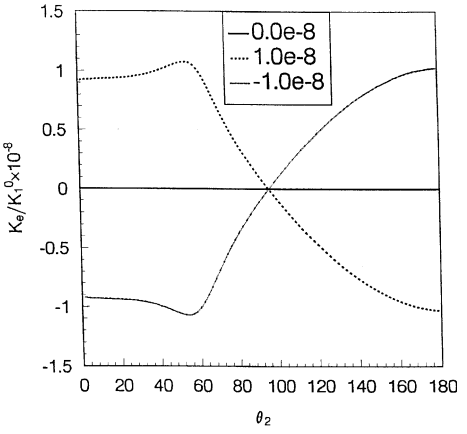

Fig. 8. Normalized EDIF at tip B of crack 2, K_e/K_I^0, plotted as a function of its orientation angle of crack 2, θ_2, for type (i), (ii), and (iii) loading conditions ($D_2^\infty/\sigma_{22}^\infty = 0$, 10^{-8}, $-10^{-8}C/N$, respectively).

parallel both to the poling direction of the piezoelectric material and to the direction of remote electric loading. However, no such electric neutral angle exists in Fig. 7 for tip A since crack 1 is always perpendicular to the poling direction as well as the electric loading direction.

5. Conclusions

Based on the results presented in this paper, the following conclusions can be summarized:

(1) The J_2-integral in piezoelectric materials can be divided into two separated parts, corresponding to the mechanical and electric quantities, although both are coupled in the constitutive equations of the materials.

(2) The conservation laws (3) and (4) found in non-piezoelectric materials also hold for piezoelectric materials. In other words, the total contributions to both components of the J_k-vector due to a cloud of randomly distributed, interacting microcracks in 2-D-piezoelectric materials vanish, provided that the closed contour along which the integration is performed encloses all the microcracks (or, equivalently, no other discontinuities exist outside of the closed contour).

(3) The conservation laws (3) and (4) can be used as a powerful tool to check the validity of numerical results and the corresponding numerical methods for strongly interacting multiple crack problems in piezoelectric materials, although they only provide two necessary conditions rather than sufficient conditions.

(4) The remote electric displacement loading has significant influence on the magnitudes of crack tip SIFs and EDIF. However, the trends exhibited by the SIFs at each crack tip subjected to combined mechanical and electric loading are similar to those under pure mechanical loading.

(5) Positive and negative electric loadings impose opposite effects on crack tip SIFs for interacting cracks. The influence is strongly non-linear due to crack interaction, depending on the relative locations and orientations of the cracks. For certain crack arrays, a positive electric loadings increases the crack tip SIFs whereas a negative electric loading decreases the crack tip SIFs. The reverse is true for other crack arrays. In general, both electric and mechanical loadings can have profound effects on crack tip SIFs: neither can be neglected.

(6) In contrary to the crack tip SIFs, the effect of remote electric loadings on crack tip EDIF is linear, because the remote mechanical loadings have little or no influence on EDIF. However, in the presence of remote electric loadings (positive or negative), the variation trends exhibited by the EDIF as the positions and orientations of the cracks are varied are rather complicated, depending strongly on the orientation of each crack relative to the poling direction of the piezoelectric. Further research is needed to fully understand the mutual shielding effect in interacting cracks.

Acknowledgements

This work was sponsored by the Chinese State Key Laboratory Foundation at Xi'an Jiaotong University and was partly supported by the Royal Society K.C. Wang Fellowship. The authors wish to thank Professor J.R. Rice of Harvard University for constructive discussions during his visit to Cambridge.

References

Budiansky, B., Rice, J.R., 1973. Conservation laws and energy-release rates. ASME J. Appl. Mech. 40, 201–203.

Chen, Y.H., 2000a. *M*-integral analysis for two-dimensional solids with strongly interacting microcracks, Part I. In an infinite brittle solid. Int. J. Solids Struct. 38, 3193–3212.

Chen, Y.H., 2000b. *M*-integral analysis for two-dimensional solids with strongly interacting microcracks, Part II. In the brittle phase of a metal/ceramic bimaterial. Int. J. Solids Struct. 38, 3213–3232.

Chen, Y.H., Hasebe, N., 1998. A consistency check for strongly interacting multiple crack problem in isotropic, anisotropic, and bimaterial solids. Int. J. Fract. 89, 333–353.

Chen, Y.H., Ma, H., 1997. Explicit formulation of the J_2-integral in anisotropic materials and its application in microcrack shielding problem. Sci. Chin. (E) 40 (6), 588–596.

Chung, M.Y., Ting, T.C.T., 1996. Piezoelectric sold with an elliptic inclusion or hole. Int. J. Solids Struct. 33, 3343–3361.

Dunn, M., 1994. The effects of crack face boundary conditions on the fracture mechanics of piezoelectric solids. Engng. Fract. Mech. 48, 25–39.

Han, J.J., Chen, Y.H., 1999. Multiple parallel cracks interaction problem in piezoelectric ceramics. Int. J. Solids Struct. 36, 3375–3390.

Hao, T.-H., Shen, Z.-Y., 1994. A new electric boundary condition of electric fracture mechanics and its application. Engng. Fract. Mech. 47, 793–802.

Herrmann, A.G., Herrmann, G., 1981. On energy-release rates for a plane crack. ASME J. Appl. Mech. 48, 525–528.

Heyer, V., Schneider, G.A., Balke, H., Drescher, J., Bahr, H.A., 1998. A fracture criterion for conducting cracks in homogeneously poled piezoelectric PZT-PIC151 ceramics. Acta Mater. 46, 6615–6622.

Horii, H., Nemat-Nasser, S., 1985. Elastic field of interacting inhomogeneities. Int. J. Solids Struct. 21, 731–745.

Horii, M., Nemat-Nasser, S., 1987. Interacting microcracks near the tip in the process zone of a macrocrack. J. Mech. Phys. Solids 35, 601–629.

Pak, Y.E., 1990. Crack extension force in a piezoelectric material. ASME J. Appl. Mech. 57, 647–653.

Pak, Y.E., 1992. Linear electro-elastic fracture mechanics of piezoelectric materials. Int. J. Fract. 54, 79–100.

Pak, Y.E., Tobin, A., 1993. On electric field effects in fracture of piezoelectric materials. In: Lee, J.S., Maugin, G.A., Shino, Y. (Eds.), ASME Mechanics of Electromagnetic Materials and Structures, AMD-Vol. 161, MD-Vol. 42, pp. 51–62.

Park, S.B., Sun, C.T., 1995a. Fracture criteria for piezoelectric ceramics. J. Am. Ceram. Soc. 78, 1475–1480.

Park, S.B, Sun, C.T., 1995b. Effect of electric fields on fracture of piezoelectric ceramics. Int. J. Fract. 70, 203–216.

Park, S.B., Park, S.S., Carman, G.P., Hahn, H.T., 1998. Measuring strain distribution during mesoscopic domain reorientation in ferroelectric materials. ASME J. Engng. Mater. Tech. 120, 1–6.

Rice, J.R., 1968. A path independent integral and the approximate analysis of stain concentration by notches and cracks. ASME J. Appl. Mech. 35, 379–386.

Shido, Y., Tanaka, K., Narita, F., 1997. Singular stress and electric fields of a piezoelectric ceramic strip under longitudinal shear. Acta Mech. 120, 31–45.

Sosa, H., 1991. Plane problems in piezoelectric media with defects. Int. J. Solids Struct. 28, 491–505.

Sosa, H., 1992. On the fracture mechanics of piezoelectric solids. Int. J. Solids Struct. 29, 2613–2622.

Sosa, H., Khutoryansky, N., 1996. New development concerning piezoelectric materials with defects. Int. J. Solids Struct. 33, 3399–3414.

Suo, Z., Kuo, C.M., Barnett, D.M., Willis, J.R., 1992. Fracture mechanics for piezoelectric ceramics. J. Mech. Phys. Solids 40, 739–765.

Xu, X.-L., Rajapakse, R.K.N.D., 1999. Analytical solution for an arbitrarily oriented void/crack and fracture of piezoceramics. Acta Mater. 47, 1735–1747.